Journal of Membrane Science 737 (2026) 124493

Contents lists available at ScienceDirect

Journal of Membrane Science

journal homepage: www.elsevier.com/locate/memsci

Fabrication of low-fouling hollow fiber membranes through the immobilization of amine-functionalized microgels on a blended PES-SMA support

Maria A. Restrepo [a], Max Horn [a], Leonard Waterkamp [a], Felipe B. de S. Mendes [a,c,d], Frederike Schiszler [a], Matthias Wessling [a,b,*]

[a] Chemical Process Engineering AVT.CVT, RWTH Aachen University, Forckenbeckstraße 51, 52074 Aachen, Germany
[b] DWI - Leibniz-Institute for Interactive Materials, Forckenbeckstraße 50, 52074 Aachen, Germany
[c] Brazilian Navy Research Institute, Rio de Janeiro, Brazil
[d] COPPE/Chemical Engineering Program, Federal University of Rio de Janeiro, Rio de Janeiro, Brazil

ARTICLE INFO

Keywords:
Styrene-maleic anhydride/polyethersulfone membrane
Antifouling
Microgel coating
Surface modification

ABSTRACT

This study presents a novel and straightforward method for fabricating low-fouling hollow fiber membranes by immobilizing amine-functionalized microgels on the membrane surface. Poly(*N*-isopropylacrylamide)-based microgels incorporating 2-aminoethyl methacrylate hydrochloride were synthesized to introduce amine functionality. The hollow fiber membrane support was fabricated from a blend of polyethersulfone (PES) and styrene–maleic anhydride (SMA), enabling covalent microgel attachment via imide bond formation under mild alkaline conditions, or through the electrostatic interaction between carboxylic acid groups in SMA and amine groups in the microgels. Membranes were characterized by scanning electron microscopy, zeta potential measurements, and pure water permeability, confirming successful microgel immobilization. Antifouling properties were assessed using static protein adsorption and cyclic constant-flux filtration experiments with bovine serum albumin and gelatin. Microgel-coated membranes exhibited markedly improved resistance to both reversible and irreversible fouling compared to unmodified membranes. While enhanced surface charge contributed to electrostatic repulsion in PES-SMA membranes, the superior performance of microgel-coated membranes under near-isoelectric and high-salinity conditions suggests that steric and hydration-layer-based barriers play a dominant role in fouling resistance. These findings underscore the effectiveness of microgel coatings and the versatility of SMA as a functional additive for scalable fabrication of antifouling membranes.

1. Introduction

Fouling is ubiquitous in membrane processes. It occurs when retained solutes accumulate on the membrane surface, leading to a decline in membrane performance over time. Regular mechanical cleaning methods, such as bubble scoring or backwashing, can effectively address reversible fouling [1]. However, irreversible fouling requires extensive chemical cleaning for its removal [2]. Although necessary, cleaning leads to prolonged downtime, increased maintenance labor, additional chemical costs, and a shortened membrane lifespan [1–3]. This has led to significant efforts to improve materials and process design to minimize fouling, particularly in water treatment, food, and pharmaceutical applications [4–6]. A major cause of irreversible fouling is the interaction between hydrophobic compounds - such as proteins, lipids, and natural organic matter- and hydrophobic polymers commonly used in membranes, such as polyethersulfone (PES) and polyvinylidene fluoride (PVDF) [7–10]. Enhancing membrane hydrophilicity is recognized as an effective strategy for improving fouling resistance [4,11].

Hydrophilicity can be enhanced by coating membranes with hydrophilic additives such as polyelectrolytes, polydopamine, nanoparticles, and zwitterionic polymers [4,12,13]. More recently, microgels have attracted attention as promising antifouling agents [14–18]. Microgels are three-dimensional, cross-linked hydrophilic polymer networks of colloidal size that can absorb large volumes of water, substantially increasing their mass and volume [19]. Beyond their inherent hydrophilicity, microgels offer a level of structural and functional tunability that sets them apart from other type of coatings: by adjusting monomer composition, cross-linker content and reaction conditions, one can precisely control particle size and mesh density; copolymerization even allows the formation of core–shell architectures

* Correspondence to: Forckenbeckstraße 51, 52074 Aachen, Germany.
E-mail address: manuscripts.cvt@avt.rwth-aachen.de (M. Wessling).

https://doi.org/10.1016/j.memsci.2025.124493
Received 19 May 2025; Received in revised form 25 July 2025; Accepted 26 July 2025
Available online 5 August 2025

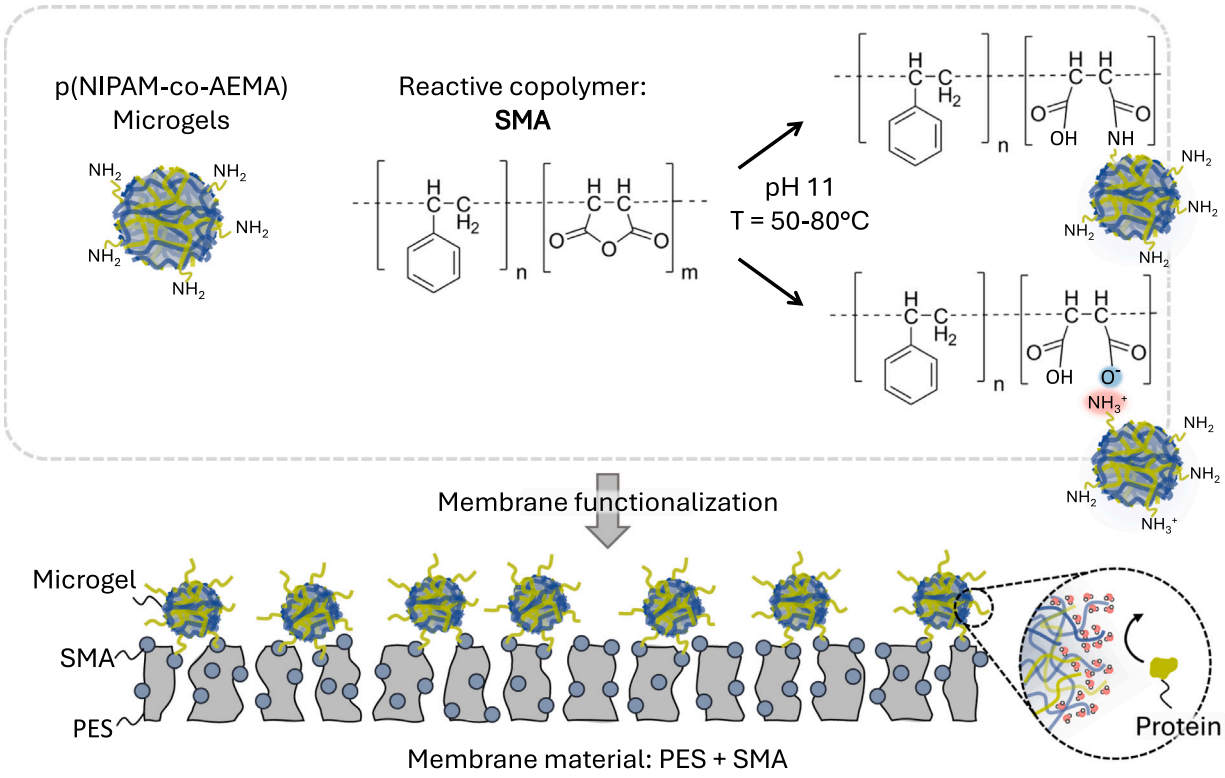

Fig. 1. Chemical structure of the p(NIPAM-co-AEMA) microgels and the schematic representation of the microgel immobilization process.

with distinct chemistries in the inside versus the outside layers [20]. For example, p(N-isopropylacrylamide) (pNIPAM)-based microgel swell below and collapse above their lower critical solution temperature, a feature already used to tune membrane permeability and molecular weight cut-off in real time [21,22]. Their three-dimensional hydrogel network also provides a convenient reservoir for enzymes, catalysts or affinity ligands [20,23], opening the door to truly multifunctional membranes [24–26].

However, lab-scale microgel synthesis by precipitation polymerization typically requires time-consuming dialysis and freeze-drying to remove unreacted monomers and surfactants. Nevertheless, continuous-flow polymerization methods coupled with membrane-based purification (e.g. ultrafiltration) are emerging as scalable routes to large-quantity, high-purity microgels [27–29].

To ensure the long-term stability of a microgel coating, the layer should ideally be covalently attached or strongy adsorbed (e.g. via electrostatic interactions) to the membrane surface, as like other hydrophilic additives, microgels are susceptible to detachment during membrane operation [30–32]. This can be accomplished by cross-linking functional groups between the microgels and the membrane surface [24], or by creating a strong electrostatic bond between the membrane support and the functional coating [31]. However, polymers commonly used in membrane fabrication, such as PES or PVDF, often lack the necessary functional groups. Therefore, the membrane surface still requires pre-treatment, which typically involves the use of harmful chemicals or time-consuming processes [4,13].

An alternative to membrane pre-treatment involves blending suitable copolymers directly into the membrane matrix, thereby facilitating subsequent surface functionalization. For instance, the copolymer styrene–maleic anhydride (SMA) blends readily with polymers such as PES or PVDF to form porous membranes [33,34]. SMA contains a hydrophobic styrene moiety, which anchors the copolymer within the hydrophobic membrane matrix [35], and a maleic anhydride moiety, which is highly reactive toward nucleophiles, enabling straightforward post-functionalization [36]. Notably, SMA has been employed to immobilize polyelectrolytes and zwitterionic polymers, enabling the fabrication of nanofiltration and low-fouling membranes [35,37–40].

In this study, we introduce a novel method for fabricating low-fouling hollow fiber membranes by coating amine-functionalized microgels to the membrane surface. Fig. 1 conceptualizes the microgel-immobilization process explored in this work. pNIPAM-based microgels were synthesized using the co-monomer 2-aminoethyl methacrylate hydrochloride (AEMA), which introduces amine functionality. A blend of PES and SMA was used to fabricate the hollow fiber support. After membrane fabrication, the membranes are immersed in a solution containing the microgels. In weak alkaline environments, the anhydride groups in the SMA react with the amine groups to form an imide bond. Alternatively, the maleic anhydride group can also undergo ring opening in alkaline environments, leading to the formation of negatively charged carboxylic acid groups [41]. The positively charged amine groups in the microgels can then interact with the negatively charged carboxylic acid groups, forming strong electrostatic bonds. To demonstrate the antifouling properties of the modified membranes, we test the membranes in extensive fouling experiments ranging from static protein adsorption to cyclic constant flux filtration with different types of proteins.

2. Experimental

2.1. Materials

For the microgel synthesis, the monomer *N*-isopropylacrylamide (NIPAM) (>98%) and the initiator 2,2-Azobis(2-methylpropionamidine) dihydrochloride (AMPA) were purchased from TCI. The cross-linker *N,N′*-methylenebis(acrylamide) (BIS) and the surfactanct cetyltrimethylammonium bromide (CTAB) were obtained from Sigma-Aldrich. The co-monomer AEMA was supplied from Polyscience. Before use, NIPAM was recrystallized in hexane (99%, VWR) and dryed under vacuum. To purify the microgel solutions, 14 kDa dialysis membranes were purchased from Carl Roth.

Table 1
Composition of polymer and bore solutions used for membrane fabrication.

Solution	PES wt.%	SMA wt.%	PVP K17 wt.%	PVP K30 wt.%	PEG 400 wt.%	NMP wt.%	DI water wt.%
PES-SMA	17.5	2	16	4	4	56.5	–
PES	17.5	–	16	4	4	58.5	–
Bore	–	–	–	–	10	60	30

Table 2
Spinning parameters used for membrane fabrication.

Parameter	Unit	Value
Temperature bore	°C	RT
Temperature polymer	°C	30
Temperature coagulation bath	°C	40
Temperature spinneret	°C	RT
Flow rate polymer	mL min^{-1}	3.6
Flow rate bore	mL min^{-1}	0.8
Air gap height	cm	16.5
Pulling wheel speed	m min^{-1}	6.8

For hollow fiber fabrication, PES (Ultrason E6020 P) and polyvinylpyrrolidone K17 (PVP K17) (M_W~10 kDa) were supplied by BASF. The SMA-copolymer XIRAN®SZ30010 (MW~10 kDa), was kindly provided by Aurorium. Polyvinylpyrrolidone K30 (M_W~40 kDa) and polyethylenglycol (M_W~400Da) were purchased from Carl Roth. The solvent *N*-methyl-2-pyrrolidone (NMP) (99%) was obtained from Fisher Scientific.

For the fouling experiments, the proteins bovine serum albumin (BSA) (heat shocked fractioned, >98%), albumin–fluorescein isothiocyanate conjugate (f-BSA), and gelatin from porcine skin (gel strength 300, type A) were purchased from Sigma-Aldrich. Phosphate buffered saline (PBS) was obtained from TH Geyer.

2.2. Hollow fiber spinning and module construction

All components required for the preparation of the polymer and bore solutions, as well as the composition of the solutions, are listed in Table 1. The polymer solution was prepared by combining all listed components in a heated glass reactor at 60 °C and mixing with a mechanical stirrer until fully dissolved. After preparation, the solution is transferred to the spinning set-up to allow it to degas overnight. The bore solution was prepared by mixing all listed components in a glass bottle with a magnetic stirrer.

Hollow fiber membranes were fabricated via a dry-jet wet phase inversion spinning technique. In this process, the polymer solution is extruded through a spinneret alongside the bore solution. Phase inversion begins upon contact with the bore solution, with partial coagulation occurring in the air gap. The hollow fibers then pass through a coagulation bath, where they solidify completely. Finally, the fibers pass through a first rinsing bath and are collected on a second rinsing bath. More detailed spinning parameters are listed in Table 2. After spinning, the fibers were immersed in DI water for 48 h to remove the remaining NMP, with an exchange of water conducted after 24 h. Then, the membranes are immersed in a 60 °C water bath for 6 h to wash out PVP from the membranes. Finally, the membranes are then placed in a bath of 50 w% glycerol/water overnight and are subsequently dried.

4-end outside-in hollow fiber modules with 58 fibers and an active length of 10 cm were manufactured using a potting centrifuge (RotaMini, Me-Sep, Poland). The resulting active membrane area was approximately 195 cm^2. Before use, the modules were flushed with DI water and filled from the inside with water using a syringe. If not in use, the modules were stored wet at room temperature.

2.3. Microgel synthesis

p(NIPAM-co-AEMA) microgels were synthesized via precipitation polymerization, following the method previously described [29]. In short, the reaction was carried out in a round-bottom flask at 80 °C under stirring at 300 rpm in a nitrogen atmosphere. The specific components were dissolved in a given volume of DI water in three separate vials. A detailed composition is listed in Table 3. The reaction starts by adding the initiator AMPA (vial 2) to a mixture of NIPAM, BIS, and the surfactant CTAB (vial 1). Two minutes into the reaction, AEMA and additional AMPA are injected (vial 3). After a total reaction time of 25 min, the polymerization is stopped by cooling the flask in ice water in the presence of oxygen. Finally, the microgels were purified using a dialysis tube.

Table 3
Recipe for the p(NIPAM-co-AEMA) microgel synthesis.

Vial	Component	Amount mg	Volume ml
1	NIPAM	220.8	–
	BIS	13.5	–
	CTAB	5.8	–
	DI-water	–	24
2	AMPA	10.6	–
	DI-water	–	3.3
3	AEMA	321.2	–
	AMPA	26.5	–
	DI-water	–	2.7

Table 4
Overview of membranes characterized in this study.

Membrane	Base polymer	Modification
P-0	PES	–
PS-0	PES-SMA	–
MG-60C	PES-SMA	0.5 mg mL^{-1} microgel at 60 °C
MG-80C	PES-SMA	0.5 mg mL^{-1} microgel at 80 °C

2.4. Membrane modification

For membrane modification, a microgel solution with a concentration of 0.5 mg/mL and a pH of 11 is obtained by diluting it with sodium hydroxide (NaOH). The concentration of the initial microgel solution was previously determined by freeze-drying a defined volume of the solution and weighing the amount of dried microgels. For the coating, the shell side of the hollow fiber modules is flushed and filled with the microgel solution. The filled modules are then submerged in a temperature-controlled water bath for 5 min at 60 or 80 °C. After the coating process, the modules are thoroughly rinsed and stored in DI-water. An overview of all types of membranes with their respective modification are listed in Table 4.

2.5. Membrane characterization

2.5.1. Pure water permeability

The pure water permeability (PWP) of the modules is measured before and after coating, and in between fouling experiments. First, water is permeated in dead-end from the shell to the lumen of the fiber at 1 bar transmembrane pressure (TMP) for at least 20 min. A scale continuously records the weight of the permeate produced. To ensure the validity of the results, the PWP is measured twice for each module.

2.5.2. Field emission scanning electron microscopy

Scanning electron microscopy (SEM) imaging was used to analyze the morphology of the membranes. Samples were fractured in liquid nitrogen to obtain cross-sectional images. Surface images were obtained by cutting the membrane samples lengthwise. A Hitachi SU5000 was used to obtain the images.

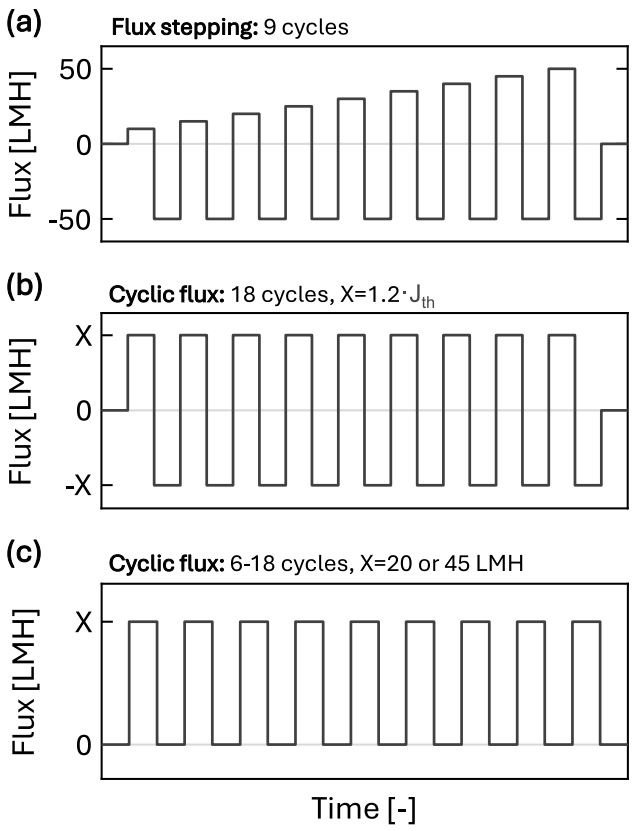

Fig. 2. (a) Flux stepping filtration method, (b) cyclic filtration at constant flux with backwashing method, and (c) cyclic filtration at constant flux with relaxation method.

2.5.3. Zeta potential

The surface zeta potential of flat sheet membranes was determined by a SurPASS analyzer (Anton Paar, Graz Austria) in a pH range of 2–9 with a 1 mM KCl electrolyte solution. The pH is automatically adjusted by two solutions of 0.1 M HCl and 0.1 M NaOH.

2.6. Fouling analysis

Three types of fouling experiments were conducted to investigate the antifouling properties of different membranes: Flux stepping, cyclic fouling at constant flux, and static fouling experiments. An automatized filtration set-up was used for the flux stepping and the cyclic fouling experiments (OSMO Poseidon, Demcon convergence, The Netherlands). A qualitative representation of the sequence of the dynamic filtration experiments is showcased in Fig. 2.

2.6.1. Flux stepping fouling

To characterize the antifouling behavior of the membranes, it is essential to examine their performance at permeate fluxes where severe fouling occurs. Such conditions arise when the permeate flux exceeds the threshold flux (J_{th}). Accordingly, J_{th} was determined for all modified and unmodified membranes through flux stepping experiments. Prior to filtration, the membranes were flushed with deionized (DI) water for 5 min to eliminate air bubbles from the module.

Subsequently, nine constant-flux filtration cycles were carried out using a model fouling solution (BSA, 0.5 g L^{-1} in PBS, pH 7.4). The initial flux was set at 10 LMH and increased in 5 LMH increments with each step. Each cycle began with a 4 min flushing step using the feed solution to fully saturate the module and tubing. This was followed by a 25 min constant-flux filtration step at the target value, and finally a 10 min backwashing step at 50 LMH using DI water. All modules were operated in an outside-in configuration under cross-flow mode, with the feed flow rate maintained at 4 kg h^{-1}.

2.6.2. Cyclic fouling at $1.2 \cdot J_{th}$ with backwashing

The sequence begins by flushing with DI-water for 5 min. Each filtration step commenced with a 4 min flush using the model fouling solution (BSA, 0.5 g L^{-1} in PBS, pH 7.4), after which the permeate flux was set to $1.2 \cdot J_{th}$ for the respective membrane. The total permeate collected per cycle was 180 g, resulting in cycle durations that varied according to each membrane's threshold flux.

Following each permeation step, a backwashing step was performed using DI water at a flux of $1.2 \cdot J_{th}$. During each backwash, 90 g of DI water was passed through the membrane. A total of 18 filtration cycles were performed per membrane. All modules operated in an outside-in configuration under cross-flow mode, with a consistent feed flow rate of 4 kg h^{-1}.

2.6.3. Cyclic fouling at constant flux with relaxation

These experiments were conducted in a manner similar to that previously described. However, the backwashing steps in the sequence are replaced by relaxation steps. The model fouling solution consists of either dissolved BSA or gelatin type A (0.5 g L^{-1} in PBS pH 7.4). Filtration steps are conducted at 45 LMH and 20 LMH for BSA and gelatin, respectively. The duration of the permeation is set to produce 180 g of permeate. The relaxation steps are equivalent to flushing the module with DI water at a feed flux of 4 kg h^{-1} for 10 min. When BSA is used as the foulant, 18 filtration cycles are conducted. When gelatin is used, only 8 cycles are conducted. The modules are operated outside-in in cross-flow mode. The feed flow rate during permeation is set at 4 kg h^{-1}.

2.6.4. Evaluation of static protein adsorption via fluorescence microscopy

Static fouling measurements were conducted to qualitatively evaluate the antifouling properties of microgel-coated membranes. Fluorescein isothiocyanate-labeled bovine serum albumin (f-BSA) served as the reference foulant and was adsorbed onto the membranes.

Flat sheet membranes with a diameter of 15 mm were placed in a 24-well plate. Before the adsorption, the membranes were thoroughly rinsed with 2 mL PBS buffer (pH 7.4). Then, 2 mL f-BSA solution with a concentration of 50 mg mL^{-1} in PBS buffer were added to each well. The adsorption took place for 3 h. The well plate was wrapped in aluminum foil to protect the fluorescein marker from bleaching. Subsequently, the membranes were again rinsed with 2 mL PBS buffer as previously described. The membranes were placed between two microscope slides, and any air bubbles were removed. The samples were wrapped once more in aluminum foil and stored at 5 °C until further analysis. The fluorescein marker on the BSA enables the evaluation with a fluorescence microscope (BZ-X810, Keyence Deutschland GmbH, Germany). All images were taken with the same exposure settings.

3. Results and discussion

3.1. Membrane fabrication and modification

Hollow fiber membrane fabrication was carried out using a dry–wet jet spinning process. A polymer solution comprising PES, SMA, and various pore-forming additives was extruded into a water coagulation bath. To achieve an outside-in fiber morphology, a bore solution primarily composed of NMP was employed. The detailed compositions of the polymer and bore solutions, along with the spinning parameters, are provided in Section 2.2. A baseline modification temperature of 60 °C was selected, as this is a typical temperature range in which SMA–amine cross-linking is performed in similar works [37,40]. To investigate whether a higher temperature would further enhance microgel attachment, we carried out parallel coatings at 80 °C. It is expected that with increasing temperature, the reaction rate between primary amines and SMA will increase [42]. Following fabrication, the membranes were modified according to the conditions described in Section 2.4. SEM images illustrating the hollow fiber morphology

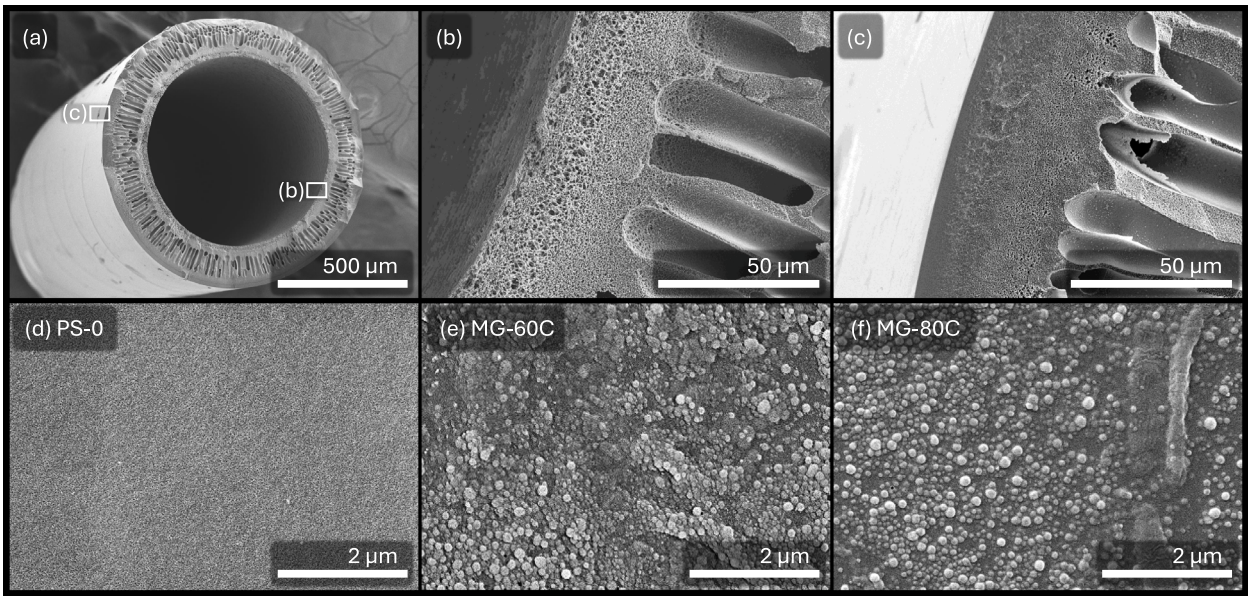

Fig. 3. Cross-sectional SEM images of the PS-0 hollow fiber membranes, and images of the shell surface before and after microgel immobilization.

and the effect of microgel modification on the membrane surface are presented in Fig. 3.

Cross-sectional SEM images of the membranes (a–c) reveal an asymmetric structure, consisting of a dense layer on the shell side, an open-porous region on the lumen side, and finger-like macrovoids in the fiber's midsection. The surface of the selective shell layer in the unmodified PS-0 membrane (d) displays small surface pores. In contrast, the MG-60C and MG-80C membranes show deposition of spherical aggregates with diameters ranging between 80 to 200 nm, which fully cover the surface pores. Prior characterization of the microgels revealed an average hydrodynamic radius of 160 nm, with a broad size distribution (PDI = 0.47) (see Supplementary Information). The wide size range observed in SEM is consistent with the large PDI. Note that the hydrodynamic radii measured are larger than the dry-state sizes seen in SEM, as microgels swell significantly in aqueous environments. This observation indicates successful microgel immobilization. No significant morphological differences were observed between the two coating temperatures (see Fig. 3(e) and (f)).

3.2. Surface properties of microgel coated membranes

As discussed in Section 3.1, an apparent deposition of a microgel layer is observed following the coating process. To elucidate the impact of this microgel layer on membrane surface properties, zeta potential and PWP measurements were conducted on unmodified PES-SMA membranes (PS-0) and microgel-modified PES-SMA membranes (MG-60C and MG-80C). For comparison, unmodified PES membranes (P-0) were also evaluated.

Fig. 4(a) shows the zeta potential of flat-sheet membranes as a function of pH. P-0 membranes exhibit a negative surface potential, as expected for unmodified PES [35]. Incorporating SMA as a copolymer (PS-0) results in a further decrease in zeta potential, particularly above pH 4, due to deprotonation of carboxylic acid groups in SMA, which typically occurs around pH 4–5. In contrast, microgel-modified membranes (MG-60C and MG-80C) display a positive shift in zeta potential, with distinctly positive values observed at pH < 5. This shift reflects the protonation of primary amines in the p(NIPAM-co-AEMA) microgels. Notably, MG-80C exhibits a more pronounced positive zeta potential than MG-60C, suggesting a higher density of immobilized microgels on its surface.

PWP measurements (Fig. 4(b)) further support the successful deposition of microgels. The PS-0 membrane exhibits a PWP of approximately 100 LMH/bar. Following microgel coating, PWP decreases by roughly 60 % and 80 % for MG-60C and MG-80C, respectively. The larger reduction observed for MG-80C aligns with its higher zeta potential, indicating a greater microgel loading. The P-0 membrane shows a PWP comparable to that of PS-0, consistent with the similar polymer solution compositions used in their fabrication.

Our results demonstrate the clear deposition of a microgel layer. However, it is not yet clear which mechanism leads to the attachment of the microgels to the membrane support. As presented in Fig. 1, we theorize microgels are immobilized either by the covalent attachment of primary amine groups to the SMA via imide bond formation, or by the electrostatic interaction between hydrolyzed SMA and the positively charged microgels. Regardless of the mechanism, we expect the interaction between SMA and the microgels to be strong enough to sustain demanding filtration cycles.

3.3. Threshold flux determination

Fouling and fouling rate are directly dependent on the applied permeate flux. This relationship is commonly described using two key parameters: the critical flux (J_{crit}) and the threshold flux (J_{th}). The critical flux is defined as the permeate flux below which no fouling occurs [43], while the threshold flux denotes the flux below which the fouling rate remains constant; above this threshold, the rate of fouling increases significantly [44,45]. Both J_{crit} and J_{th} are influenced by membrane properties, hydrodynamic conditions, and other process variables [44].

Flux stepping experiments are widely used to determine both J_{crit} and J_{th} [46,47]. In these experiments, the flux is incrementally increased and held constant for a fixed duration at each step. Key experimental parameters (including step length, step height, feed composition, and flow conditions) significantly affect fouling behavior and, consequently, the flux thresholds observed [48]. To minimize carryover effects from previous steps, intermediate cleaning protocols can be implemented between filtration cycles [47,49]. However, due to the extended durations required to accurately determine J_{crit} [44,47], flux stepping is more commonly employed for identifying J_{th} [45,47].

The membranes examined in this study differ substantially in intrinsic filtration resistance and surface charge, which are expected to influence their fouling behavior under comparable filtration conditions. To evaluate the antifouling performance of microgel-coated

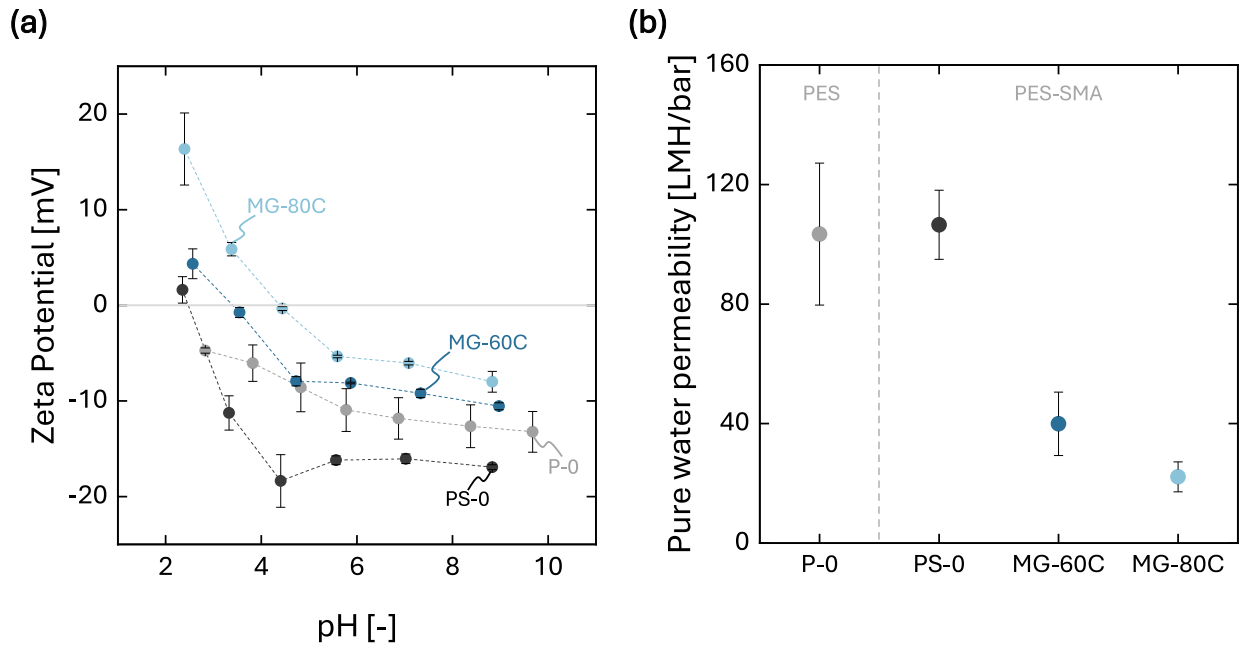

Fig. 4. Effect of microgel immobilization on (a) the zeta potential of the membranes, and (b) on the pure water permeability (PWP). As reference, a membrane fabricated without SMA as additive (P-0) is included.

Table 5
Resulting J_{th} of the different membranes evaluated.

Membrane	$J_{th,a}$ LMH	$J_{th,b}$ LMH	$J_{th,c}$ LMH	$1.2 \cdot J_{th,a}$ LMH
P-0	**33**	25	20	**40**
PS-0	**28.3**	25	25	**34**
MG-60C	**22.1**	20	20	**27**
MG-80C	**16.6**	15	15	**20**

membranes, all samples were tested at fluxes exceeding their respective J_{th}, ensuring that fouling effects were sufficiently pronounced.

Flux stepping experiments were conducted to determine J_{th} for each membrane type. The applied flux was increased in 5 LMH increments from 10 LMH to 50 LMH, BSA as the model foulant. Each filtration step was followed by a backwashing cycle with deionized water. During each step, the evolution of TMP was recorded over time. Three TMP-based metrics were extracted to determine J_{th}: the average TMP per step (TMP_{avg}), the stepwise change in TMP (ΔTMP), and the TMP gradient over time ($d(TMP)/d(t)$). These values were plotted as a function of flux, and J_{th} was estimated according to the methodology described by Miller et al. [45].

The results of these experiments are presented in Fig. 5. Three distinct fouling regimes were observed for the P-0, PS-0, and MG-60C membranes: (1) a regime with negligible TMP increase (10 LMH–20 LMH); (2) a plateau region in TMP (25 LMH–35 LMH); and (3) a regime characterized by a sharp increase in TMP with each step (40 LMH–50 LMH). For MG-60C, domains 2 and 3 appear to shift slightly to lower flux values. However, the presence of domain 1 in all three membrane types confirms that their J_{th} values lie within the tested flux range. In contrast, for the MG-80C membrane, only domains 2 and 3 were observed, suggesting a lower J_{th}, though its precise value could not be determined due to the system's minimum flux setting of 10 LMH.

Table 5 lists the resulting J_{th} for the methods using (a) TMP_{avg}, (b) ΔTMP, (c) $d(TMP)/d(t)$. Only the values of J_{th} determined by TMP_{avg} are considered, as this method gives the highest value of J_{th}. Subsequent experiments use the rounded values of $1.2 \cdot J_{th}$ calculated using $J_{th,a}$.

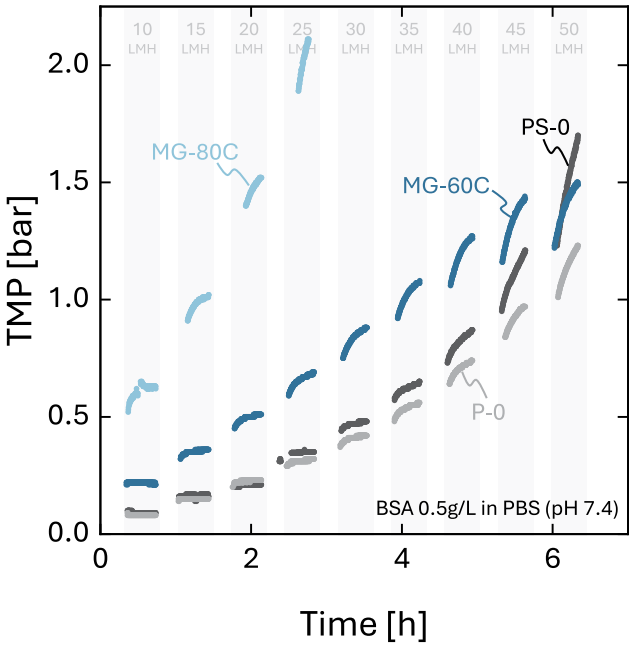

Fig. 5. Flux stepping experiments with unmodified PES and PES-SMA hollow fiber membranes, and modified PES-SMA hollow fiber membranes with 0.5 g L^{-1} BSA as the model foulant. The flux was increased from 10 LMH to 50 LMH in 5 LMH steps. Each step had a duration of 25 min and was followed by a 10 min backwashing step.

3.4. Cyclic fouling at constant flux with BSA

To evaluate the impact of membrane modification on antifouling performance, constant-flux filtration experiments were conducted at $1.2 \cdot J_{th}$ for each membrane (see Table 5), and at a fixed flux of 45 LMH/bar. Each experiment comprised 18 filtration cycles. For tests at $1.2 \cdot J_{th}$, a backwashing step at the same flux was performed between cycles. In contrast, for the 45 LMH experiments, only relaxation steps were applied between cycles. A detailed description of the methodology can be found in Section 2.6.

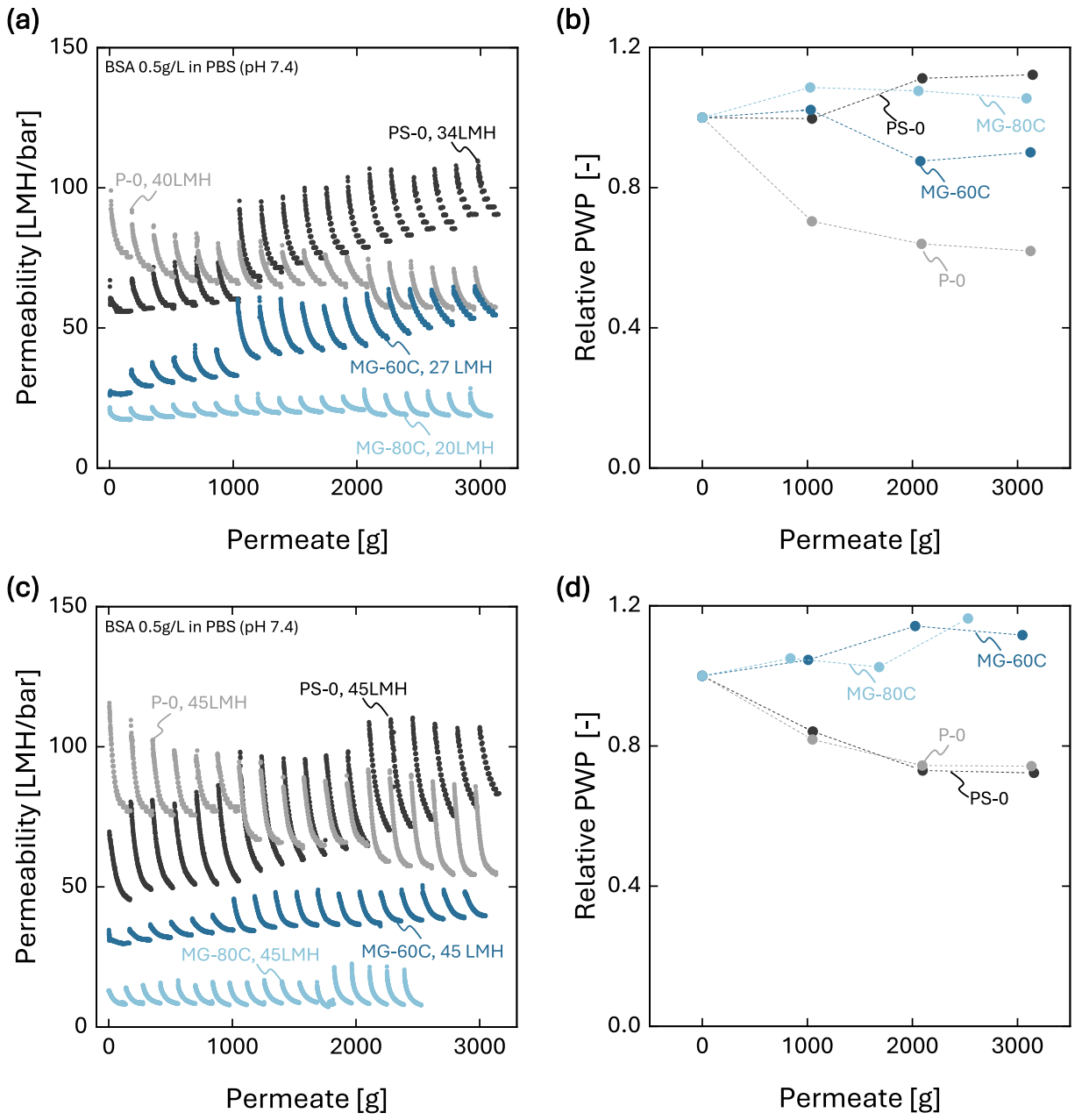

Fig. 6. Fouling behavior of unmodified and modified hollow fiber membranes after 18 cycles of 0.5 g L^{-1} BSA filtration at constant flux. Reversible fouling was measured as a function of the decline of permeability over the produced permeate. Irreversible fouling was characterized by the change in the pure water permeability of the membranes in between 6 cycles. (a) Fouling experiments conducted at $1.2 \cdot J_{th}$ with backwashing, and (b) the corresponding pure water permeability of membranes in-between cycles. (c) Fouling experiments conducted at 45 LMH with relaxation steps in-between cycles, and (d) the corresponding pure water permeability.

Before each filtration cycle, the modules were rinsed with the BSA solution to ensure complete saturation of the internal volume. Due to initial pressure losses in the module, a low TMP is temporarily established, resulting in an unregulated permeation phase during which fouling may occur. Consequently, the permeability measured at the beginning of each step may not accurately represent the true post-cleaning permeability of the membrane. To quantify irreversible fouling, the relative loss of PWP was assessed every six cycles. The results of these experiments are presented in Fig. 6, with subfigures (a) and (b) corresponding to $1.2 \cdot J_{th}$, and (c) and (d) corresponding to a constant flux of 45 LMH.

The cyclic fouling experiments conducted at $1.2 \cdot J_{th}$ revealed predominantly reversible fouling behavior in each filtration cycle for the PS-0, MG-60C, and MG-80C membranes. Notably, PS-0 and MG-60C exhibited a gradual increase in final permeability across cycles, whereas the P-0 membrane showed a continuous decline in final permeability, consistent with trends observed in the PWP measurements. In contrast, PS-0, MG-60C, and MG-80C did not display a significant reduction in PWP over the 18 cycles, indicating minimal to no irreversible fouling.

The progressive increase in final permeability observed for PS-0 and MG-60C may suggest a reduced adsorption of BSA on the membrane surface over time, as indicated by the stable PWP. This effect could be attributed to enhanced electrostatic repulsion between the negatively charged BSA molecules and the increasingly negative membrane surface [10,50,51]. SMA may undergo further ring-opening hydrolysis under physiological pH conditions [52], which increases surface charge density. Although SMA in MG-60C membranes was initially activated via immersion in diluted NaOH at 60 °C, further hydrolysis may have occurred in the PBS buffer during filtration. For MG-80C, this effect

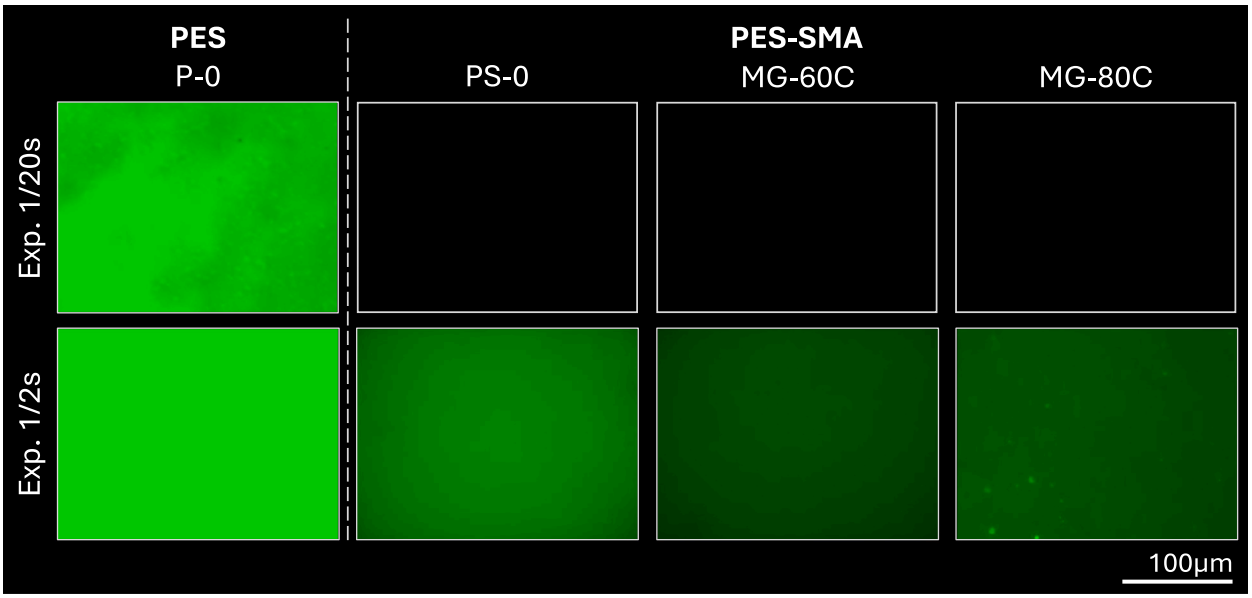

Fig. 7. Static BSA adsorption on unmodified and modified PES-SMA flat sheet membranes. An unmodified PES membrane is used as a reference. Two light exposure times (1/20 s and 1/2 s) are used to demonstrate the significantly lower adsorption of all PES-SMA membranes compared with membranes prepared only with PES. At a longer exposure time, slightly higher protein adsorption can be observed for the PS-0 membrane compared to other PES-SMA membranes.

may be suppressed by the presence of a thicker microgel layer, which likely shields the membrane surface (see Section 3.2).

At the higher flux of 45 LMH, the observed fouling behavior followed similar trends. The P-0 membrane exhibited a progressive decline in final permeability, indicative of irreversible fouling, which was further confirmed by decreasing PWP values across cycles. In contrast, both PS-0 and MG-60C showed increasing final permeability over time, with the effect being more pronounced for PS-0. The MG-80C membrane demonstrated a stable permeability profile throughout the 18 cycles, although it produced less permeate overall due to difficulty in maintaining the set flux. Due to the high TMP required for MG-80C, the system was unable to rapidly reach the target flux, which reduced the effective filtration time at the set flux. Post-experimental PWP measurements confirmed the absence of irreversible fouling for MG-60C and MG-80C, while PS-0 exhibited a reduction in PWP, suggesting partial accumulation of BSA.

Concluding, the cyclic-flux experiments with BSA not only demonstrate the antifouling function of the microgel coating but also its mechanical robustness. Even after 18 consecutive cycles (11.4 h of continuous protein filtration and cleaning) at $1.2 \cdot J_{th}$ with backwashing or at 45 LMH—both well above the J_{th} of the microgel-coated membranes—the PWP recovers fully after the cleaning steps. Such reproducible recovery provides direct evidence that the microgel layer remains stable and active throughout extended operation. Although this testing duration is on par with published studies of other SMA-based antifouling membranes [37–39], future work will focus on testing the functionality and stability of microgel-coated membranes under more industry-relevant conditions. For example, during multi-day operation and using fluxes below the membranes' J_{th}.

3.5. Evaluation of static BSA adsorption

Static adsorption experiments using f-BSA were conducted on flat-sheet membranes to corroborate the cyclic fouling experiments. Static adsorption was achieved by immersing membrane samples in a f-BSA solution under continuous shaking. Afterward, the membranes were washed with a buffer solution, and the degree of adsorption was qualitatively evaluated based on the intensity of the fluorescent signal captured by a fluorescence microscope. A higher fluorescent signal indicates more significant BSA adsorption. The results are presented in Fig. 7.

All PES-SMA membranes exhibited no visible coloration at short exposure times (1/20 s), in stark contrast to the bright green appearance of the unmodified PES membrane. At a longer exposure time (1/2 s), a slightly more intense coloration was observed for the PS-0 membrane compared to MG-60C and MG-80C. This may indicate a higher fouling tendency for the unmodified PES-SMA membrane. However, based on the full set of experimental results, it can only be concluded with certainty that all PES-SMA membranes—irrespective of modification—exhibit low affinity for BSA. This observation is consistent with previous reports on the low BSA affinity of PES-SMA blended membranes [35]. These findings are further supported by the dynamic fouling experiments. For PS-0, the low fouling behavior can be attributed to electrostatic repulsion between the negatively charged membrane surface and BSA, which has an isoelectric point (IEP) between 4.1 and 4.7 [53]. In the case of MG-60C and MG-80C, it remains unclear whether the immobilized microgel layer further enhances this effect through the formation of a hydration barrier on the membrane surface.

3.6. Cyclic fouling at constant flux with gelatin

Cyclic filtration experiments with BSA demonstrated that microgel-modified membranes exhibit enhanced antifouling properties, particularly under high-flux conditions. However, it remains unclear whether this low affinity for BSA is primarily due to electrostatic repulsion between the protein and the membrane surface, or to the formation of a robust hydration layer provided by the microgel coating. To further investigate this, additional experiments were conducted using gelatin type A. Gelatin type A has an IEP between pH 7 and 8 [54], and is therefore expected to be neutral or slightly positively charged under the experimental conditions (PBS buffer, pH 7.4).

The fouling experiments followed the same protocol as previously described, employing six cyclic filtration cycles at constant flux using a gelatin solution (0.5 g L^{-1} in PBS buffer). Relaxation steps with water were applied between cycles. An initial flux of 45 LMH was tested, but resulted in complete permeability loss for the PS-0 membrane during the first cycle. Consequently, a reduced flux of 20 LMH was used for the remainder of the experiments. The results are presented in Fig. 8.

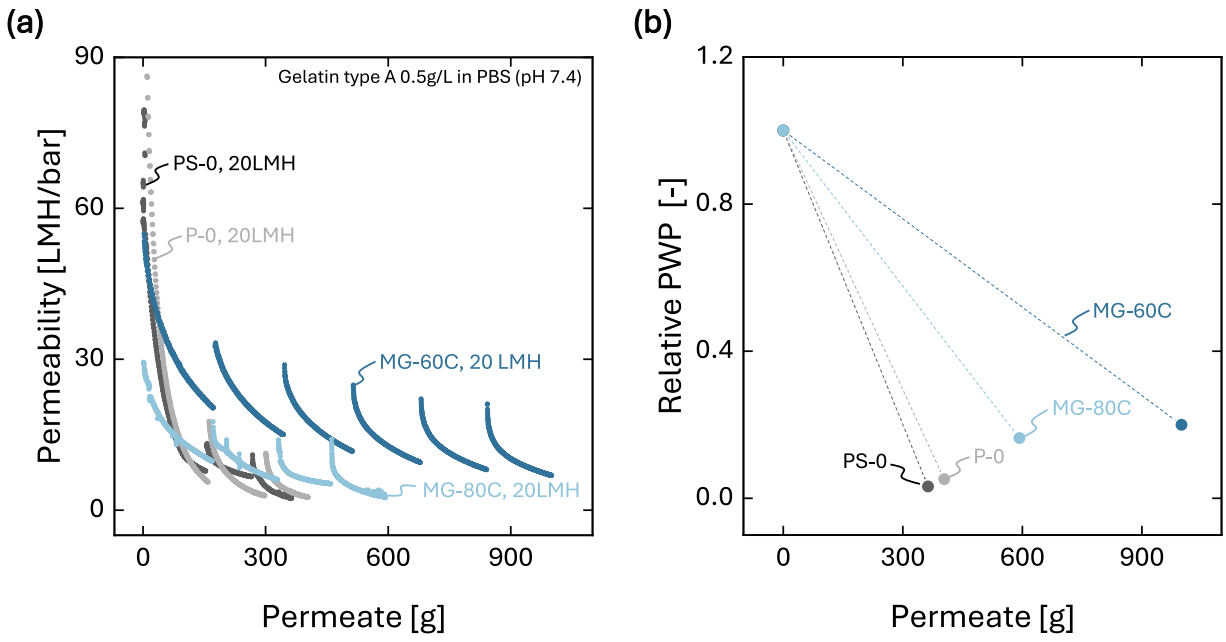

Fig. 8. Fouling behavior of unmodified and modified hollow fiber membranes after 6 cycles of 0.5 g L^{-1} Gelatin filtration at 20 LMH. (a) Permeability decline as a function of the produced permeate. (b) Relative pure weater permeability before and after the fouling experiments.

In general, more pronounced fouling was observed with gelatin compared to BSA, which is consistent with literature findings that protein fouling is most severe near the protein's IEP [55–57]. Proteins exhibit increased hydrophobicity at their IEP, promoting stronger adsorption to membrane surfaces via hydrophobic interactions [11]. Moreover, after the formation of a protein monolayer, the absence of electrostatic repulsion between protein molecules can further exacerbate fouling [55]. This tendency is further amplified by gelatin's own structure. The gelatine used (gel strength 300) consist of a mixture of collagen fragments ranging between 50–100 kDa in size [58] that adopt a random-coil conformation with exposed hydrophobic domains near its IEP [51]. The combination of chain flexibility and increased hydrophobicity drives the rapid formation of a cohesive gel layer [59]. Under the high TMPs used here (up to 5 bar), this film compacts into a dense network that may resists detachment, even in the presence of a robust hydration barrier.

Distinct fouling behaviors were observed among the membranes. Both microgel-coated membranes experienced fouling, but exhibited less severe permeability loss than the unmodified membranes (P-0 and PS-0). MG-60C completed all six filtration cycles before reaching the TMP limit of 5 bar, whereas experiments with P-0, PS-0, and MG-80C were terminated early due to excessive TMP. After the first cycle and subsequent relaxation, MG-60C and MG-80C retained approximately two-thirds of their initial permeability. In contrast, PS-0 lost roughly 90% of its initial permeability during the first cycle, with minimal recovery after relaxation. In subsequent cycles, MG-60C and MG-80C showed improved stability, as demonstrated by noticeable permeability recovery following each relaxation step.

No clear correlation was found between surface charge and fouling severity. This is illustrated by the similar fouling behavior of P-0 and PS-0, despite the more negative zeta potential of PS-0 (see Fig. 4(a)). Additionally, MG-60C outperformed MG-80C even though MG-80C exhibited a more positive zeta potential. This discrepancy may be attributed to the lower initial permeability of MG-80C. In the case of P-0 and PS-0, the substantial loss in permeability likely results from their more hydrophobic nature. Indeed, Huisman et al. [11] demonstrated that stronger hydrophobic interactions between membrane surfaces and proteins lead to more significant initial permeability losses during constant-pressure filtration. In contrast, electrostatic interactions did not correlate with the decline in permeability at any stage.

Thus, our results suggest that the improved antifouling performance of microgel-coated membranes is driven by to two complementary mechanisms: electrostatic repulsion and hydration layer formation. While PS-0 membranes benefited primarily from increased negative surface charge introduced by SMA, which electrostatically repels negatively charged proteins like BSA, the microgel-coated membranes (MG-60C and MG-80C) appear to leverage an additional, dominant effect: the formation of a robust hydration barrier. Hydration layers act as a physical and energetic barrier to protein adsorption by creating a shell of tightly bound water molecules around the membrane surface, which proteins must displace to adhere. This mechanism is less sensitive to pH and ionic strength than electrostatic repulsion and is therefore especially effective under near-isoelectric or high-salinity conditions [60], such as those present in the gelatin fouling tests. Our results support this interpretation: despite the reduced surface charge of MG-80C and MG-60C, their fouling resistance under gelatin filtration conditions remained superior to that of PS-0, suggesting that hydration-layer-based steric hindrance played a dominant role. These findings are consistent with previous research, which highlights hydration-layer formation—especially via hydrophilic and zwitterionic coatings—as one of the most effective and universal strategies for long-term antifouling performance in protein-rich and variable-salinity environments [60].

Moreover, while the significant increase in hydraulic resistance imposed by the microgel layer may be seen as a significant drawback of the microgel coating, this effect must be weighed against gains in long-term stability under heavy protein fouling. In highly demanding processes—such as in the biotech dairy industry, where feeds contain complex, high-concentration protein mixtures—a slightly reduced initial flux can be compensated by dramatically extended run times, far fewer cleaning cycles, and longer membrane lifetimes. In such settings, a robust hydration layer barrier that trades some permeability for sustained performance may yield higher net throughput and lower total life-cycle cost than a pristine but rapidly fouling membrane.

Finally, it is worth noting that the gelatin fouling protocol is not as well optimized as the BSA tests. As shown in Fig. 8(a), fouling proceeds so quickly at 20 LMH that this flux clearly exceeds the J_{th} of all membrane types, as the fouling rate is also dependent on the type of protein used [7,50,51]. In future work, we will refine the gelatin protocol by first performing flux-stepping to determine each

membrane's J_{th}, then running cyclic fouling at more moderate fluxes. Even under these harsh conditions, however, our results highlight how critical foulant choice is when evaluating the hydrophilic properties of modified membranes.

4. Conclusion

This study presents a straightforward method for fabricating low-fouling hollow fiber membranes by coating amine-functionalized p(NIPAM-co-AEMA) microgels to the membrane surface. A membrane support composed of a blend of PES and SMA enables the subsequent immobilization of microgels without the use of harsh chemicals or complex procedures. PES-SMA membranes were coated at 60 °C and 80 °C, referred to as MG-60C and MG-80C, respectively. For comparison, unmodified PES and PES-SMA membranes (P-0 and PS-0, respectively) were also evaluated.

SEM images confirmed the formation of a uniform microgel layer on the membrane surface, while zeta potential measurements showed a positive shift consistent with the introduction of amine groups from the microgels. A decrease in PWP was observed for the microgel-coated membranes, consistent with the presence of a hydrophilic microgel layer. Flux stepping experiments were used to determine the threshold flux of the different membranes. In cyclic filtration tests using BSA as the model foulant, the microgel-modified membranes maintained higher permeability over multiple cycles compared to the unmodified membranes. The unmodified PS-0 membrane also outperformed the P-0 membrane, which was attributed to enhanced electrostatic repulsion between the negatively charged BSA and the more negatively charged PS-0 surface. These findings were supported by static protein adsorption experiments using fluorescently labeled BSA, which showed substantially lower protein adsorption on both unmodified PES-SMA and microgel-coated membranes.

Additional cyclic fouling experiments with gelatin type A—a protein with an isoelectric point near the experimental pH—further confirmed the superior antifouling performance of the microgel-coated membranes. Under these conditions, the unmodified membranes rapidly lost permeability and were unable to complete the filtration cycles, whereas the microgel-modified membranes retained functionality and completed the test protocol. These results highlight the effectiveness of microgel coatings in improving membrane fouling resistance, even under challenging conditions where electrostatic effects are minimized.

Overall, our approach offers a practical and scalable strategy for enhancing the antifouling performance of hollow fiber membranes. The covalent attachment or strong adsorption of functionalized microgels ensures a stable surface modification capable of withstanding operational conditions without significant loss of the coating. Nonetheless, solutions to the current limitations regarding the increase in hydraulic resistance by the addition of the microgel layer should be explored in the future. For instance, fabricating a support with a higher initial PWP may counteract the permeability loss from the microgel layer. Additionally, fine-tuning the coating conditions (for example, by lowering the reaction temperature or using more dilute microgel dispersions) can limit excess deposition while maintaining full coverage. Furthermore, the microgel structure can also be tuned in terms of particle size, cross-link density, or amine content to achieve a balance between transport and fouling resistance. Finally, future work could also explore the multifunctional character of microgels, for example, by incorporating bioactive molecules—such as proteins or enzymes—into the microgels or utilizing their stimuli-responsive properties, enabling the development of antifouling and biofunctional membranes for specialized applications in the biomedical, food, and beverage industries

CRediT authorship contribution statement

Maria A. Restrepo: Writing – review & editing, Writing – original draft, Visualization, Validation, Supervision, Project administration, Methodology, Investigation, Formal analysis, Conceptualization. **Max Horn:** Writing – original draft, Visualization, Validation, Methodology, Investigation, Formal analysis, Conceptualization. **Leonard Waterkamp:** Writing – original draft, Visualization, Validation, Methodology, Investigation, Formal analysis, Conceptualization. **Felipe B. de S. Mendes:** Writing – review & editing, Validation, Supervision, Methodology, Conceptualization. **Frederike Schiszler:** Methodology, Investigation, Formal analysis. **Matthias Wessling:** Writing – review & editing, Writing – original draft, Visualization, Validation, Supervision, Resources, Funding acquisition, Conceptualization.

Declaration of Generative AI and AI-assisted technologies in the writing process

During the preparation of this work, ChatGPT was used to refine writing and enhance readability. The authors thoroughly reviewed and edited the AI-generated content as necessary, and take full responsibility for the content of this publication.

Declaration of competing interest

The authors declare that they have no known competing financial interests or personal relationships that could have appeared to influence the work reported in this paper.

Acknowledgments

The authors would like to thank Karin Faensen for the high-quality FESEM. This work was supported by the Industrial Collective Research (IGF) under the projekt "Selbstreinigende Hohlfasermembranen mit enzymatisch aktiven Mikrogelen" (22894 N). M.W. acknowledges the DFG funding through the Gottfried Wilhelm Leibniz Award 2019 (WE 4678/12-1). M.W. appreciates the support from the Alexander-von-Humboldt foundation, Germany.

Appendix A. Supplementary data

Supplementary material related to this article can be found online at https://doi.org/10.1016/j.memsci.2025.124493.

Data availability

Data will be made available on request.

References

[1] K.V. Peinemann, S.P. Nunes, Membranes for Water Treatment, Wiley-VCH ; [John Wiley, distributor], 2010, p. 237.
[2] W. Guo, H.H. Ngo, J. Li, A mini-review on membrane fouling, Bioresour. Technol. 122 (2012) 27–34, http://dx.doi.org/10.1016/j.biortech.2012.04.089.
[3] X. Shi, G. Tal, N.P. Hankins, V. Gitis, Fouling and cleaning of ultrafiltration membranes: A review, J. Water Process. Eng. 1 (2014) 121–138, http://dx.doi.org/10.1016/j.jwpe.2014.04.003.
[4] D. Rana, T. Matsuura, Surface modifications for antifouling membranes, Chem. Rev. 110 (2010) 2448–2471, http://dx.doi.org/10.1021/cr800208y.
[5] B. Díez, R. Rosal, A critical review of membrane modification techniques for fouling and biofouling control in pressure-driven membrane processes, Nanotechnol. Environ. Eng. 2020 5:2 5 (2020) 1–21, http://dx.doi.org/10.1007/s41204-020-00077-x.
[6] B.V.D. Bruggen, Chemical modification of polyethersulfone nanofiltration membranes: A review, J. Appl. Polym. Sci. 114 (2009) 630–642, http://dx.doi.org/10.1002/app.30578.

[7] C. Zhang, Q. Bao, H. Wu, M. Shao, X. Wang, Q. Xu, Impact of polysaccharide and protein interactions on membrane fouling: Particle deposition and layer formation, Chemosphere 296 (2022) 134056, http://dx.doi.org/10.1016/j.chemosphere.2022.134056.

[8] M. Hadidi, A.L. Zydney, Fouling behavior of zwitterionic membranes: Impact of electrostatic and hydrophobic interactions, J. Membr. Sci. 452 (2014) 97–103, http://dx.doi.org/10.1016/j.memsci.2013.09.062.

[9] K. Xiao, X. Wang, X. Huang, T.D. Waite, X. Wen, Combined effect of membrane and foulant hydrophobicity and surface charge on adsorptive fouling during microfiltration, J. Membr. Sci. 373 (2011) 140–151, http://dx.doi.org/10.1016/j.memsci.2011.02.041.

[10] J. Wang, H. Wang, L. Shen, R. Li, H. Lin, A sustainable solution for organic pollutant degradation: Novel polyethersulfone/carbon cloth/FeOCl composite membranes with electric field-assisted persulfate activation, Water Res. 244 (2023) 120530, http://dx.doi.org/10.1016/j.watres.2023.120530.

[11] I.H. Huisman, P. Prádanos, A. Hernández, The effect of protein–protein and protein–membrane interactions on membrane fouling in ultrafiltration, J. Membr. Sci. 179 (2000) 79–90, http://dx.doi.org/10.1016/S0376-7388(00)00501-9.

[12] Z. Yan, Y. Zhang, H. Yang, G. Fan, A. Ding, H. Liang, G. Li, N. Ren, B.V. der Bruggen, Mussel-inspired polydopamine modification of polymeric membranes for the application of water and wastewater treatment: A review, Chem. Eng. Res. Des. 157 (2020) 195–214, http://dx.doi.org/10.1016/j.cherd.2020.03.011.

[13] R. Zhang, Y. Liu, M. He, Y. Su, X. Zhao, M. Elimelech, Z. Jiang, Antifouling membranes for sustainable water purification: Strategies and mechanisms, Chem. Soc. Rev. 45 (2016) 5888–5924, http://dx.doi.org/10.1039/c5cs00579e.

[14] C. Aksoy, P. Kaner, A. Asatekin, P.Z. Çulfaz-Emecen, Co-deposition of stimuli-responsive microgels with foulants during ultrafiltration as a fouling removal strategy, ACS Appl. Mater. Interfaces 11 (2019) 18711–18719, http://dx.doi.org/10.1021/acsami.9B03217.

[15] S. Maity, B. Mishra, K. Nayak, N.C. Dubey, B.P. Tripathi, Zwitterionic microgel based anti(-bio)fouling smart membranes for tunable water filtration and molecular separation, Mater. Today Chem. 24 (2022) 100779, http://dx.doi.org/10.1016/j.mtchem.2022.100779.

[16] S. Maity, D. Gaur, B. Mishra, N.C. Dubey, B.P. Tripathi, Bactericidal and biocatalytic temperature responsive microgel based self-cleaning membranes for water purification, J. Colloid Interface Sci. 642 (2023) 129–144, http://dx.doi.org/10.1016/j.jcis.2023.03.095.

[17] B. Mishra, S. Biswal, N.C. Dubey, B.P. Tripathi, Anti(-bio)fouling nanostructured membranes based on the cross-linked assembly of stimuli-responsive zwitterionic microgels, ACS Appl. Polym. Mater. 4 (2022) 4719–4733, http://dx.doi.org/10.1021/acsapm.2C00302.

[18] X. Chen, S. Bi, C. Shi, Y. He, L. Zhao, L. Chen, Temperature-sensitive membranes prepared from blends of poly(vinylidene fluoride) and poly(N-isopropylacrylamides) microgels, Colloid Polym. Sci. 291 (2013) 2419–2428, http://dx.doi.org/10.1007/S00396-013-2985-Y.

[19] M. Karg, A. Pich, T. Hellweg, T. Hoare, L.A. Lyon, J.J. Crassous, D. Suzuki, R.A. Gumerov, S. Schneider, I.I. Potemkin, W. Richtering, Nanogels and microgels: From model colloids to applications, recent developments, and future trends, Langmuir 35 (2019) 6231–6255, http://dx.doi.org/10.1021/acs.langmuir.8B04304.

[20] F.A. Plamper, W. Richtering, Functional microgels and microgel systems, Acc. Chem. Res. 50 (2017) 131–140, http://dx.doi.org/10.1021/acs.accounts.6B00544.

[21] M. Barth, M. Wiese, W. Ogieglo, D. Go, A.J.C. Kuehne, M. Wessling, Monolayer microgel composite membranes with tunable permeability, J. Membr. Sci. 555 (2018) 473–482, http://dx.doi.org/10.1016/j.memsci.2018.03.037.

[22] D.J. Bell, S. Ludwanowski, A. Lüken, B. Sarikaya, A. Walther, M. Wessling, Hydrogel membranes made from crosslinked microgel multilayers with tunable density, J. Membr. Sci. 620 (2021) 118912, http://dx.doi.org/10.1016/j.memsci.2020.118912.

[23] M. Nöth, E. Gau, F. Jung, M.D. Davari, I. El-Awaad, A. Pich, U. Schwaneberg, Biocatalytic microgels (μ-Gel zymes): Synthesis, concepts, and emerging applications, Green Chem. 22 (2020) 8183–8209, http://dx.doi.org/10.1039/d0gc03229h.

[24] G. Vitola, D. Büning, J. Schumacher, R. Mazzei, L. Giorno, M. Ulbricht, Development of a novel immobilization method by using microgels to keep enzyme in hydrated microenvironment in porous hydrophobic membranes, Macromol. Biosci. 17 (2017) 1600381, http://dx.doi.org/10.1002/mabi.201600381.

[25] K. Ogawa, B. Wang, E. Kokufuta, Enzyme-regulated microgel collapse for controlled membrane permeability, Langmuir 17 (2001) 4704–4707, http://dx.doi.org/10.1021/la0102354.

[26] H. Zhang, J. Luo, Y. Wan, Regenerable temperature-responsive biocatalytic nanofiltration membrane for organic micropollutants removal, ISc. 25 (2022) http://dx.doi.org/10.1016/j.isci.2021.103671.

[27] A. Lüken, M. Bruckhaus, U. Kosfeld, M. Emondts, M. Wessling, Automated tangential-flow diafiltration device, HardwareX 10 (2021) e00200, http://dx.doi.org/10.1016/j.ohx.2021.e00200.

[28] H.J. Wolff, M. Kather, H. Breisig, W. Richtering, A. Pich, M. Wessling, From batch to continuous precipitation polymerization of thermoresponsive microgels, ACS Appl. Mater. Interfaces 10 (2018) 24799–24806, http://dx.doi.org/10.1021/acsami.8B06920.

[29] F.B. de S. Mendes, P. Saha, F.M. F., D. Zafar, J. Rubner, M. Wessling, C.P. Borges, H. Roth, Scalable fabrication of amine-functionalized microgel composite membranes and their gas permeation characteristics, J. Membr. Sci. 692 (2024) 122315, http://dx.doi.org/10.1016/j.memsci.2023.122315.

[30] M. Wiese, T. Lohaus, J. Haussmann, M. Wessling, Charged microgels adsorbed on porous membranes - A study of their mobility and molecular retention, J. Membr. Sci. 588 (2019) 117190, http://dx.doi.org/10.1016/j.memsci.2019.117190.

[31] J. de Grooth, B. Haakmeester, C. Wever, J. Potreck, W.M. de Vos, K. Nijmeijer, Long term physical and chemical stability of polyelectrolyte multilayer membranes, J. Membr. Sci. 489 (2015) 153–159, http://dx.doi.org/10.1016/j.memsci.2015.04.031.

[32] T. Miyano, T. Matsuura, D.J. Carlsson, S. Sourirajan, Retention of polyvinylpyrrolidone swelling agent in the poly(ether p-phenylenesulfone) ultrafiltration membrane, J. Appl. Polym. Sci. 41 (1990) 407–417, http://dx.doi.org/10.1002/app.1990.070410132.

[33] T. Xiang, M. Tang, Y. Liu, H. Li, L.L. Li, W. Cao, S. Sun, C. Zhao, Preparation and characterization of modified polyethersulfone hollow fiber membranes by blending poly (styrene-alt-maleic anhydride), Desalination 295 (2012) 26–34, http://dx.doi.org/10.1016/j.desal.2012.03.021.

[34] L.P. Zhu, X.X. Zhang, L. Xu, C.H. Du, B.K. Zhu, Y.Y. Xu, Improved protein-adsorption resistance of polyethersulfone membranes via surface segregation of ultrahigh molecular weight poly(styrene-alt-maleic anhydride), Colloids Surf. B 57 (2007) 189–197, http://dx.doi.org/10.1016/j.colsurfb.2007.01.021.

[35] T. Helmecke, I.I. Rose, M.V. Tsurkan, H. Roth, M.F. Maitz, C. Werner, M. Wessling, Poly(styrene-alt-maleic anhydride)-copolymers blended in poly(ether sulfone) membranes as a platform for effective biomolecular surface functionalization, J. Membr. Sci. 689 (2024) 122050, http://dx.doi.org/10.1016/j.memsci.2023.122050.

[36] Z. Jin, L. Du, C. Zhang, Y. Sugiyama, W. Wang, G. Palui, S. Wang, H. Mattoussi, Modification of poly(maleic anhydride)-based polymers with H2N-R nucleophiles: Addition or substitution reaction? Bioconjug. Chem. 30 (2019) 871–880, http://dx.doi.org/10.1021/acs.bioconjchem.9B00008.

[37] J. Jin, X. Du, J. Yu, S. Qin, M. He, K. Zhang, G. Chen, High performance nanofiltration membrane based on SMA-PEI cross-linked coating for dye/salt separation, J. Membr. Sci. 611 (2020) 118307, http://dx.doi.org/10.1016/j.memsci.2020.118307.

[38] D. Hu, H. Zhao, G. Feng, M. Xu, C. Wang, Y. Li, Fabrication of nanofiltration membranes through the deposition of polyethyleneimine on SMA-polyethersulfone supports under acid catalysis for cationic dye/salt separation, J. Environ. Chem. Eng. 11 (2023) 111055, http://dx.doi.org/10.1016/j.jece.2023.111055.

[39] Y.C. Lin, C.M. Chao, D.K. Wang, K.M. Liu, H.H. Tseng, Enhancing the antifouling properties of a PVDF membrane for protein separation by grafting branch-like zwitterions via a novel amphiphilic SMA-HEA linker, J. Membr. Sci. 624 (2021) 119126, http://dx.doi.org/10.1016/j.memsci.2021.119126.

[40] P. Zhang, S. Rajabzadeh, T. Istirokhatun, Q. Shen, Y. Jia, X. Yao, A. Venault, Y. Chang, H. Matsuyama, A novel method to immobilize zwitterionic copolymers onto PVDF hollow fiber membrane surface to obtain antifouling membranes, J. Membr. Sci. 656 (2022) 120592, http://dx.doi.org/10.1016/j.memsci.2022.120592.

[41] A.H. Kopf, M.C. Koorengevel, C.A. van Walree, T.R. Dafforn, J.A. Killian, A simple and convenient method for the hydrolysis of styrene-maleic anhydride copolymers to styrene-maleic acid copolymers, Chem. Phys. Lipids 218 (2019) 85–90, http://dx.doi.org/10.1016/j.chemphyslip.2018.11.011.

[42] H.Y. Liu, K. Cao, Y. Huang, Z. Yao, B.G. Li, G.H. Hu, Kinetics and simulation of the imidization of poly(styrene-co-maleic anhydride) with amines, J. Appl. Polym. Sci. 100 (2006) 2744–2749, http://dx.doi.org/10.1002/app.23371.

[43] R.W. Field, D. Wu, J.A. Howell, B.B. Gupta, Critical flux concept for microfiltration fouling, J. Membr. Sci. 100 (1995) 259–272, http://dx.doi.org/10.1016/0376-7388(94)00265-z.

[44] R.W. Field, G.K. Pearce, Critical, sustainable and threshold fluxes for membrane filtration with water industry applications, Adv. Colloid Interface Sci. 164 (2011) 38–44, http://dx.doi.org/10.1016/j.cis2010.12.008.

[45] D.J. Miller, S. Kasemset, L. Wang, D.R. Paul, B.D. Freeman, Constant flux crossflow filtration evaluation of surface-modified fouling-resistant membranes, J. Membr. Sci. 452 (2014) 171–183, http://dx.doi.org/10.1016/j.memsci.2013.10.037.

[46] W.J. van de Ven, K.v.t. Sant, I.G. Pünt, A. Zwijnenburg, A.J. Kemperman, W.G. van der Meer, M. Wessling, Hollow fiber dead-end ultrafiltration: Influence of ionic environment on filtration of alginates, J. Membr. Sci. 308 (1–2) (2008) 218–229, http://dx.doi.org/10.1016/j.memsci.2007.09.062.

[47] A. Drews, Membrane fouling in membrane bioreactors—Characterisation, contradictions, cause and cures, J. Membr. Sci. 363 (2010) 1–28, http://dx.doi.org/10.1016/j.memsci.2010.06.046.

[48] P.L. Clech, B. Jefferson, I.S. Chang, S.J. Judd, Critical flux determination by the flux-step method in a submerged membrane bioreactor, J. Membr. Sci. 227 (2003) 81–93, http://dx.doi.org/10.1016/j.memsci.2003.07.021.

[49] P. van der Marel, A. Zwijnenburg, A. Kemperman, M. Wessling, H. Temmink, W. van der Meer, An improved flux-step method to determine the critical flux and the critical flux for irreversibility in a membrane bioreactor, J. Membr. Sci. 332 (2009) 24–29, http://dx.doi.org/10.1016/j.memsci.2009.01.046.

[50] H.J. Tanudjaja, A. Anantharaman, A.Q.Q. Ng, Y. Ma, M.B. Tanis-Kanbur, A.L. Zydney, J.W. Chew, A review of membrane fouling by proteins in ultrafiltration and microfiltration, J. Water Process. Eng. 50 (2022) 103294, http://dx.doi.org/10.1016/j.jwpe.2022.103294.

[51] Z.Z. Mustafa, N.R. Rao, R.K. Henderson, G.L. Leslie, P. Le-Clech, Considerations of the limitations of commonly applied characterisation methods in understanding protein-driven irreversible fouling, Environ. Sci.: Water Res. Technol. 8 (2022) 343–357, http://dx.doi.org/10.1039/D1EW00831E.

[52] T. Pompe, L. Renner, M. Grimmer, N. Herold, C. Werner, Functional films of maleic anhydride copolymers under physiological conditions, Macromol. Biosci. 5 (2005) 890–895, http://dx.doi.org/10.1002/mabi.200500097.

[53] B. Jachimska, M. Wasilewska, Z. Adamczyk, Characterization of globular protein solutions by dynamic light scattering, electrophoretic mobility, and viscosity measurements, Langmuir 24 (2008) 6867–6872, http://dx.doi.org/10.1021/la800548p.

[54] S. Bäther, C.S. Hundschell, H. Kieserling, A.M. Wagemans, Impact of the solvent properties on molecular interactions and phase behaviour of alginate-gelatin systems, Colloids Surfaces A: Physicochem. Eng. Asp. 656 (2023) 130455, http://dx.doi.org/10.1016/j.colsurfa.2022.130455.

[55] W.S. Ang, M. Elimelech, Protein (BSA) fouling of reverse osmosis membranes: Implications for wastewater reclamation, J. Membr. Sci. 296 (2007) 83–92, http://dx.doi.org/10.1016/j.memsci.2007.03.018.

[56] J. Ma, L. Qin, X. Zhang, H. Huang, Temporal evolution of the selectivity-permeability relationship during porous membrane filtration of protein solutions, J. Membr. Sci. 514 (2016) 385–397, http://dx.doi.org/10.1016/j.memsci.2016.05.022.

[57] Q. She, C.Y. Tang, Y.N. Wang, Z. Zhang, The role of hydrodynamic conditions and solution chemistry on protein fouling during ultrafiltration, Desalination 249 (2009) 1079–1087, http://dx.doi.org/10.1016/j.desal.2009.05.015.

[58] Sigma-Aldrich, Gelatine from porcine skin, gel strength 300, Type A, 2025, https://www.sigmaaldrich.com/deepweb/assets/sigmaaldrich/product/documents/343/638/g2500pis.pdf. (Accessed 22 July 2025).

[59] N.A. Burger, G. Meier, D. Vlassopoulos, B. Loppinet, High-pressure effects on gelatin sol-gel transition, Ind. Eng. Chem. Res. 64 (2025) 7370–7380, http://dx.doi.org/10.1021/acs.iecr.4c04861.

[60] S. Chen, L. Li, C. Zhao, J. Zheng, Surface hydration: Principles and applications toward low-fouling/nonfouling biomaterials, Polym. 51 (2010) 5283–5293, http://dx.doi.org/10.1016/j.polymer.2010.08.022.